Current Medical Science
DOI https://doi.org/10.1007/s11596-023-2755-0
43(3):526-538,2023

# DLAT as a Cuproptosis Promoter and a Molecular Target of Elesclomol in Hepatocellular Carcinoma*

Fan GAO[1], Yuan YUAN[1], Yang DING[2], Pei-yuan LI[1], Ying CHANG[2, 3#], Xing-xing HE[1, 2, 3#]
[1]*Department of Gastroenterology, Tongji Hospital, Tongji Medical College, Huazhong University of Science and Technology, Wuhan 430030, China*
[2]*Department of Gastroenterology, Zhongnan Hospital of Wuhan University, Wuhan 430071, China*
[3]*Hubei Clinical Center and Key Laboratory of Intestinal and Colorectal Diseases, Wuhan 430071, China*



**[Abstract] Objective:** Cuproptosis is a novel cell death pathway that was newly discovered in early 2022. However, cuproptosis is still in its infancy in many respects and warrants further research in hepatocellular carcinoma (HCC). This study aimed to analyze the mechanism of cuprptosis in HCC. **Methods:** Herein, the tumor microenvironment infiltration landscape of molecular subtypes was illustrated using GSVA, ssGSEA, TIMER, CIBERSORT, and ESTIMATE algorithms based on the expression profile of cuproptosis-related genes (CRGs) from TCGA and GEO databases. Then, the least absolute shrinkage and selection operator regression method was applied to construct a cuproptosis signature to quantify the cuproptosis profile of HCC. Further, we explored the expression of three hub CRGs in cell lines and clinical patient tissues of HCC by Western blotting, qRT-PCR and immunohistochemistry. Finally, we examined the function of dihydrolipoamide S-acetyltransferase (DLAT) in cuproptosis in HCC by loss-of-function strategy, Western blotting and CCK8 assay. **Results:** Three distinct molecular subtypes were identified. Cluster 2 had the greatest infiltration of immune cells with best prognosis. The cuproptosis signature was indicative of tumor subtype, immunity, and prognosis for HCC, and specifically, a low cuproptosis score foreshadowed good prognosis. DLAT was highly expressed in liver cancer cell lines and HCC tissues and positively correlated with clinical stage and grade. We also found that potent copper ionophore elesclomol could induce cuproptosis in a copper-dependent manner. Selective $Cu^{++}$ chelator ammonium tetrathiomolybdate and downregulating DLAT expression by siRNA could effectively inhibit cuproptosis. **Conclusion:** Cuproptosis and DLAT as a promising biomarker could help to determine the prognosis of HCC and may offer novel insights for effective treatment.
**Key words:** cuproptosis; hepatocellular carcinoma; tumor microenvironment; immune checkpoint; immunotherapy

Generally, the known cell death pathways include apoptosis, necroptosis, pyroptosis and ferroptosis[1]. A recent study elucidated a novel mechanism of copper-induced cell death defined as cuproptosis, which is distinct from previously-mentioned pathways and has attracted widespread attention[2]. Although copper levels are elevated in different solid tumors and are required for tumor growth and angiogenesis processes[3–7], the concentration of copper in tumor cells is only 2- to 3-fold at extraordinarily low levels compared to normal tissue[8]. The accumulation of intracellular copper is prevented from being harmful to cells through an active endostasis mechanism[9]. Studies have reported that copper ionophores resulted in a 5- to 10-fold rapid increase in intracellular copper levels, thereby disrupting the homeostasis of copper ions and leading to the development and progression of cancer[2, 10]. Emerging evidence also indicates crosstalk between copper levels and the tumor immune microenvironment. Research shows that copper supplementation enhances PD-L1 expression in cancer cells and regulates a key signaling pathway for PD-L1-driven immune evasion in cancer[11]. Inflammatory response induces intracellular copper uptake and promotes colon tumorigenesis[12]. A phase Ⅱ study demonstrated that copper scavenging with tetrathiomolybdate in high-risk recurrent breast

Fan GAO, E-mail: 2825968016@qq.com
#Corresponding author, Xing-xing HE, E-mail: hexingxing@whu.edu.cn; Ying CHANG, E-mail: changying@whu.edu.cn
*This research was financially supported by grants from the National Natural Science Foundation of China (No. 82073095, No. 82172938 and No. 81670554) and Science and Technology Innovation Cultivation Fund of Zhongnan Hospital of Wuhan University (No. CXPY2020042).
**Electronic supplementary material** The online version of this article (https://doi.org/10.1007/s11596-023-2755-0) contains supplementary material, which is available to authorized users.

cancer patients and preclinical lung metastasis models affects the tumor microenvironment (TME)[13]. Elevated copper levels in cancer cells offer promise for selective cancer therapy[14]. Copper-chelating agents that reduce the copper ions, such as trientine, could inhibit tumor development in various tumors like hepatocellular carcinoma (HCC) and could be applied in antitumor immune and anticancer treatment[11, 15–17]. However, cuproptosis is still in its infancy in many respects, and further research is urgently needed in HCC.

Primary liver cancer was the world's 6th most common cancer in 2020 and one of the three leading causes of cancer death[18]. Despite advances in treatment of HCC in recent years, the sensitivity of drug therapy is still not well-understood[19]. Considering the large incidence, there is an urgent need to develop more effective prognostic models. Three hub cuproptosis-related genes (CRGs) *LIPT1*, *DLAT*, *CDKN2A* we identified from all CRGs are mentioned in a previous article[2]. For instance, lipolytransferase1 (LIPT1), the enzyme involved in the lipoic acid pathway that catalyzes the transfer of the lipoyl group from lipoyl-AMP, has been shown to be an independent favorable prognostic indicator for melanoma patients[20]. The pyruvate dehydrogenase complex (DLAT) links the glycolytic pathway to the tricarboxylic cycle[21] and has been reported to be upregulated in gastric cancer[22]. CDKN2A, a negative regulator of tumor, is capable of inducing cell cycle arrest in G1 and G2 phases[23].

In this study, HCC samples from The Cancer Genome Atlas (TCGA) were classified into three subtypes associated with cuproptosis based on 10 CRGs. Multiple algorithms were used to explore the differences in tumor immune infiltration between these subtypes. In this study, a cuproptosis signature was developed and the key cuproptosis gene, *DLAT*, was identified as a promising new biomarker for prognosis and intervention treatment.

## 1 MATERIALS AND METHODS

### 1.1 Data Sources

RNA expression (FPKM and raw counts) and the relevant prognostic and clinicopathological data for HCC were downloaded from the Gene Expression Omnibus (GEO, https://www.ncbi.nlm.nih.gov/geo/), the University of California Santa Cruz (UCSC, https://xena.ucsc.edu/), and TCGA (https://portal.gdc.cancer.gov/) databases. We obtained 371 HCC patients with clinical information from TCGA, among which 369 HCC patients had expression data. And 209 HCC patients were obtained from GEO. GEO HCC cohorts (GSE14520) and TCGA HCC cohorts were obtained for subsequent analyses. GSE14520 data were log2-transformed and manually normalized with the "limma" package. The chip probes were mapped into human gene symbols by using the "Bioconductor" package. Finally, normal tissue samples and samples without clinical information were excluded.

### 1.2 Unsupervised Clustering for CRGs

First, we identified 10 CRGs from a previous publication[2]. Then, the 369 cases of HCC from TCGA were classified into different molecular subtypes using R package "ConsensusClusterPlus" based on expression levels of these 10 genes. The GSE14520 cohort from GEO was used to validate the accuracy. We performed 1000 replications to ensure the stability of the classification.

### 1.3 Functional and Pathway Enrichment Analysis

The gene sets "c2.cp.kegg.v7.5.1.symbols.gmt" were downloaded from the Molecular Signature Database (MSigDB, http://software.broadinstitute.org/gsea/msigdb/index.jsp). To investigate the differences among the different cuproptosis clusters in biological processes, we used the R package "Gene Set Variation Analysis (GSVA)" to calculate the score of each patient based on previously-defined Kyoto Encyclopedia of Genes and Genomes (KEGG) pathways. Subsequently, the R package "limma" was used to compare the GSVA scores of different cuproptosis clusters. Pathways with $P$ value <0.2 were considered as significantly altered[24].

### 1.4 Correlations between Cuproptosis Cluster and TME

The score of TME cells was assessed using single-sample Gene Set Enrichment Analysis (ssGSEA) algorithm. For reliable immune characterization, we used CIBERSORT (https://cibersort.stanford.edu/) to evaluate the relative fraction of 22 immune cells based on "LM22" file provided by the official website. We performed 50 calculations to obtain the relative ratio of the 22 immune cells[25]. The R package based on the ESTIMATE algorithm was also used to calculate the immune, ESTIMATE, stromal, and tumor purity scores.

### 1.5 Identification of Cuproptosis Prognostic Signature

To explore whether CRGs are indicative of prognosis of HCC, four CRGs were found to be associated with prognosis by univariate Cox analysis ($P$<0.05). Then, R package "glmnet" was used to perform regression analysis with the LASS-COX method[26]. In addition, we set up a 10-fold cross-validation to obtain the optimal model. We set the lambda value to 0.021928873016607, and three hub genes and their correlative coefficients were obtained. A predicted cuproptosis score formula was established as follows: cuproptosis score = $\Sigma$(Expi×Coefi), where Coefi and Expi denote the risk coefficient and expression of each gene, respectively. The optimal cut-off value was calculated using the surv_cutpoint function in the R package "Survminer". Finally, model sensitivity and specificity were evaluated by the

Receiver Operating Characteristic (ROC) analyses.

**1.6 Expression Analysis of three Hub CRGs**

We investigated the expression levels of three hub genes between tumor and normal samples using GEPIA2 (http://gepia2.cancer-pku.cn) and UALCAN (http://ualcan.path.uab.edu/) based on TCGA samples[27]. Meanwhile, we also investigated the expression levels of three hub genes between individual cancer stage and tumor grade using UALCAN.

**1.7 Tumor Immune Estimation Resource Analysis**

Tumor Immune Estimation Resource (TIMER, https://cistrome.shinyapps.io/timer/) was used to investigate the relationship between the expression of CRGs and abundance of six immune cells ($CD4^+$ T cells, $CD8^+$ T cells, B cells, neutrophils, dendritic cells, and macrophages)[28].

**1.8 Tissue Specimens and Cell Culture**

After obtaining informed consent and following ethical and institutional guidelines, all 40 tumor and paired adjacent non-tumor liver tissue specimens were obtained from HCC patients undergoing partial hepatectomy between January 2019 and December 2020 at Zhongnan Hospital, Wuhan University. This study was approved by the Zhongnan Hospital Ethics Committee of Wuhan University (Approval No. 2022011K). All cell lines were cultured in DMEM supplemented with 10% fetal bovine serum (Cegrogen, Germany) in a humidified atmosphere with 5% $CO_2$ at 37°C.

**1.9 Western Blotting Assay**

The protein was lysed in RIPA buffer (Promoter, China) containing PMSF (Promoter, China) and protease inhibitors cocktail (MCE, USA) for 30 min on ice. Cell lysates were high-speed centrifuged for 10 min at 4°C . The supernatant was collected, and the protein concentration was determined using a BCA kit (Servicebio, China). Protein was boiled, electrophoresed, then transferred to PVDF membranes. The membranes were closed with 5% non-fat milk dissolved in TBST for 1 h. The membranes were incubated with primary antibodies at 4°C overnight. After washing the membranes with TBST 3 times, they were incubated with secondary antibodies for 1 h. The images were developed by an imaging system (Tanon 5200 Multi, China). The antibodies used in this study were as follows: anti-DLAT (Proteintech, China, 13426-1-AP), anti-LIPT1 (Aviva Systems Biology, China, ARP48785_P050), and anti-CDKN2A (Cell Signaling Technology, USA, 80772T).

**1.10 RNA Isolation and Quantitative Real-time PCR**

Total RNA was isolated by RNA-easy isolation reagent (Vazyme, China) and subjected to the reverse transcription to cDNA using HiScript® Ⅱ Q Select RT SuperMix for qPCR (Vazyme, China). QuantStudio 3 Real-Time PCR systems (Applied Biosystems, USA) were used for quantitative real-time PCR to detect the expression of RNA using Hieff® qPCR SYBR Green Master Mix (Yeasen, China). The qPCR primers were as follows: DLAT (forward 5′-CCGCCGCTATTACAGTCTTCC-3′; reverse 5′-CTCTGCAATTAGGTCACCTTCAT-3′); CDKN2A (forward 5′-ATGGAGCCTTCGGCTGACTG-3′; reverse 5′-TCATGACCTGGATCGGCCT-3′); LIPT1 (forward 5′-AAATCTGGCTGTGGAAGACTGG-3′; reverse 5′-CTCTGCAATTAGGTCACCTTCAT-3); ACTIN (forward 5′-CATGTACGTTGCTATCCAGGC-3′; reverse 5′-CC TACCAATTACAACAGAGGGAGA-3′).

**1.11 CCK8 and MTT Assay**

Cell viability was measured by a cell counting kit-8 (CCK8) assay and MTT assay. First, 2000–5000 cells were planted per well. Indicated concentrations of compounds were added 16–24 h after planting. CCK8 and MTT were measured 48 h after elesclomol (MCE, USA) addition. The cell culture medium and CCK-8 (Promoter, China) were mixed in a 10:1 ratio to incubate the cells at 37°C for 1, 2, 3, and 4 h. MTT solution was added to the cells and incubated for 4 h at 37°C, then aspirated it out and added DMSO to dissolve formazan. Then, the 450-nm and 490-nm absorbance was measured by a microplate reader. cell viability was calculated based on the absorbance value of test wells, blank drug wells, and control wells.

**1.12 Immunohistochemistry (IHC)**

Tissue sections were baked in an oven at 60°C for 30 min followed by deparaffinization and rehydration. Antigen repair was then performed with EDTA. After adding goat serum blocking solution and blocking for 20 min at room temperature, tissue sections were incubated with DLAT antibody (Proteintech, 13426-1-AP) in a ratio of 1:800 overnight at 4°C. The next day, the sections were re-warmed and incubated with secondary antibody for 1 h at room temperature. Finally, sections were incubated with DAB solution for 5 min and washed with tap water for 5 min.

## 2 RESULTS

**2.1 Identification of Cuproptosis Clusters in HCC**

Detailed clinical information of HCC patients in TCGA cohort and the Gene Expression Omnibus (GEO)-GSE14520 cohort included in this study are presented in table S1. To examine the classification of cuproptosis in HCC, we applied the method of consensus clustering based on the consensus matrix (fig. S1A and fig. 1A), the cumulative distribution function (CDF) curve (fig. S1B), and delta area curve (fig. S1C) results. When k=3, the CDF curve was smoother, close to the lowest point, and did not contain groups with small sample sizes. Finally, HCC was stratified into three clusters: 190 cases in cluster 1, 67 cases in cluster 2, and 112 cases in cluster 3 (fig. S1D). Survival

analysis showed that there were significant differences among the three cuproptosis clusters, where cluster 2 had a significant survival advantage (fig. 1B). Principal component analysis (PCA) revealed significant differences in the transcriptional profiles among the three cuproptosis clusters (fig. 1C). The expression of CRGs differed markedly between the three cuproptosis clusters (fig. 1D and 1E). The correlation between the three clusters and various clinical characteristics is also shown in fig. 1D. GSE14520 cohort was selected as the validation cohort to determine the repeatability of this clustering. As the TCGA cohort, consensus clustering analysis was performed, and again, HCC was classified into three clusters (fig. S1E–S1H). Although there was no significant difference in survival analysis among these three clusters (fig. S1I), the expression of CRGs was significantly different (fig. 1F), proving that there are three clusters of HCC.

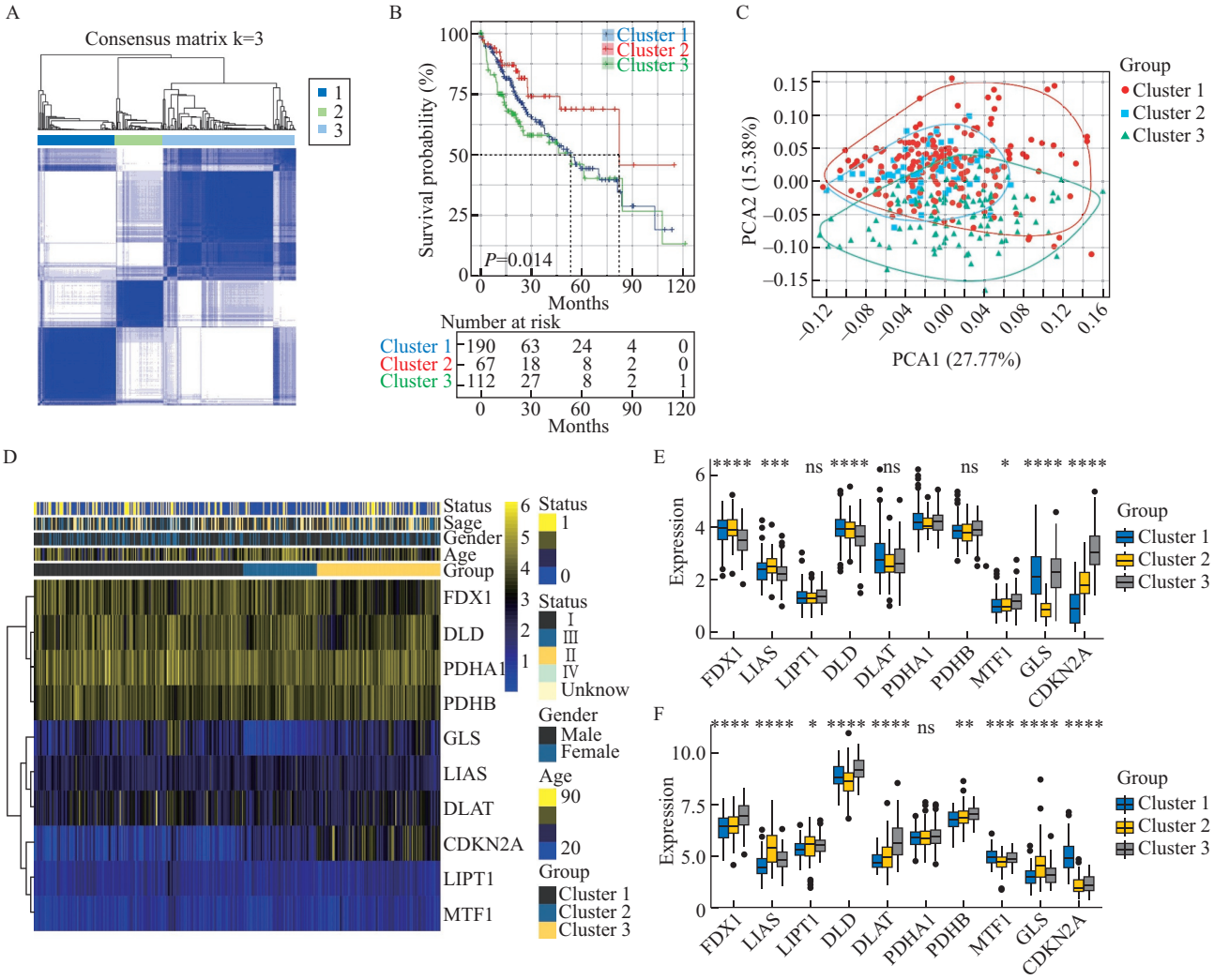


**Fig. 1** Biological characteristics of cuproptosis clusters based on cuproptosis-related genes (CRGs)
A: consensus matrix (k=3) for CRGs in The Cancer Genome Atlas (TCGA) samples ($n$=369); B: Kaplan-Meier curves showing overall survival (OS) of hepatocellular carcinoma (HCC) cuproptosis clusters in TCGA cohort; C: Principal component analysis of 10 CRGs in TCGA cohort identified three distinct subtypes; D: heatmap of 10 CRGs in TCGA cohort. Tumor stage, gender, age, survival status and cluster were used as patient annotations; E: differential expression of CRGs among three cuproptosis clusters in TCGA cohort; F: differential expression of CRGs among three cuproptosis clusters in GSE14520 cohort. The statistical differences among the three clusters were analyzed by the kruskal test. $^{*}P$<0.05, $^{**}P$<0.01, $^{***}P$<0.001, $^{****}P$<0.0001; ns: not statistically significant

## 2.2 Characteristics of TME Cell Infiltration in Cuproptosis Clusters

To explore the biological function characteristics of the three clusters, GSVA enrichment analysis was conducted. The findings showed that cluster 1 was significantly enriched in some metabolism-related pathways, including nitrogen metabolism, alanine aspartate and glutamate metabolism, and arginine and proline metabolism pathways. Cluster 2 was mainly linked to systemic lupus erythematosus, complement and coagulation cascades, and prion diseases pathways. Cluster 3 was mainly pertinent to primary immunodeficiency and the JAK-STAT signaling pathway (fig. 2A and 2B). Next, we assessed

the correlations between three cuproptosis clusters and TME using ssGSEA. We observed that gamma delta T cells, mast cells, plasmacytoid dentritic cells, type 1 T helper cells, and type 17 T helper cells made up the largest infiltration in cluster 2 (fig. 2C). Cluster 2 also had most rich immunoinfiltration. The ESTIMATE

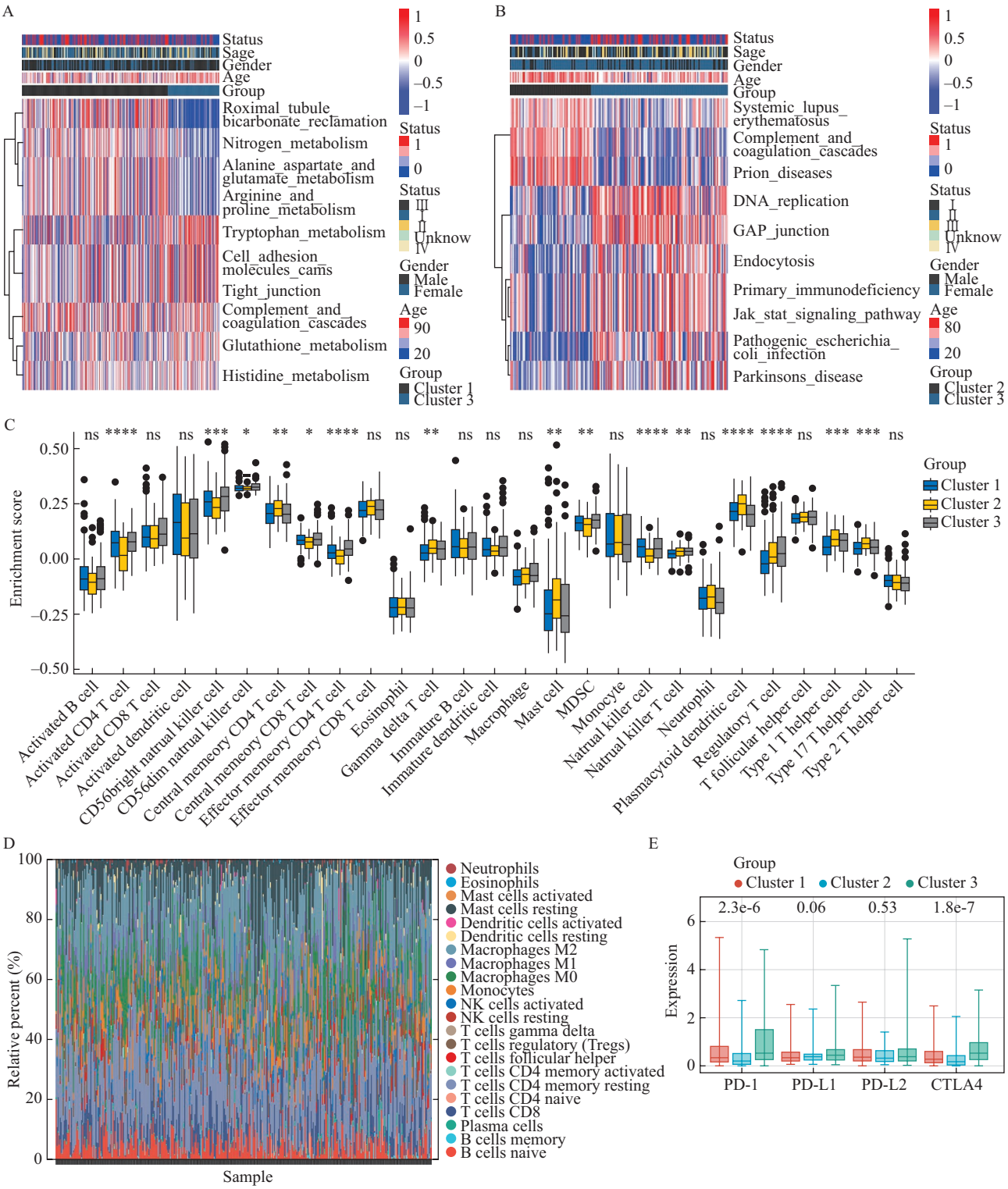


**Fig. 2** Tumor microenvironment (TME) cell infiltration and biological characteristics in three cuproptosis clusters of hepatocellular carcinoma (HCC)

A gene set variation analysis (GSVA) was done to analyze the biological pathways of three cuproptosis clusters. Cluster, tumor stage, gender, age, survival status were used as sample annotations. A: cluster 1 *vs*. cluster 2; B: cluster 2 *vs*. cluster 3; C: 27 TME cells infiltration abundance of three cuproptosis clusters; D: the relative percentage of 22 subpopulations of immune cells in 369 samples from The Cancer Genome Atlas (TCGA) cohort; E: differential expression of immune checkpoints in three cuproptosis clusters. The statistical differences among the three clusters were analyzed by the kruskal test. $^{*}P<0.05$, $^{**}P<0.01$, $^{***}P<0.001$, $^{****}P<0.0001$; ns: not statistically significant; MDSC: myeloid derived suppressor cell

score (fig. S2B) and immune score (fig. S2C) of the cuproptosis clusters were comprehensively analyzed. We found that cluster 1 scored slightly higher than cluster 2 and cluster 3. Similarly, stromal scores (fig. S2D) and tumor purity (fig. S2E) revealed the same results.

To further investigate the correlations between the three cuproptosis clusters and 22 human immune cell subsets, we performed the CIBERSORT analysis to show the relative percentage of the 22 kinds of immune cells in each patient (fig. 2D). Differences in the composition of TME-infiltrating cells were noted among the three cuproptosis clusters (fig. S2A and S2F). Expression of immune checkpoint was of significant difference among three cuproptosis clusters, where cluster 3 had the highest expression level of immune checkpoint (fig. 2E). This result proves that cuproptosis plays an important role in TME.

### 2.3 Identification of Cuproptosis Prognostic Signature

The results of univariate Cox regression identified four CRGs associated with prognosis of patients with HCC (fig. 3A). The least absolute shrinkage and selection operator (LASSO) Cox regression was used to

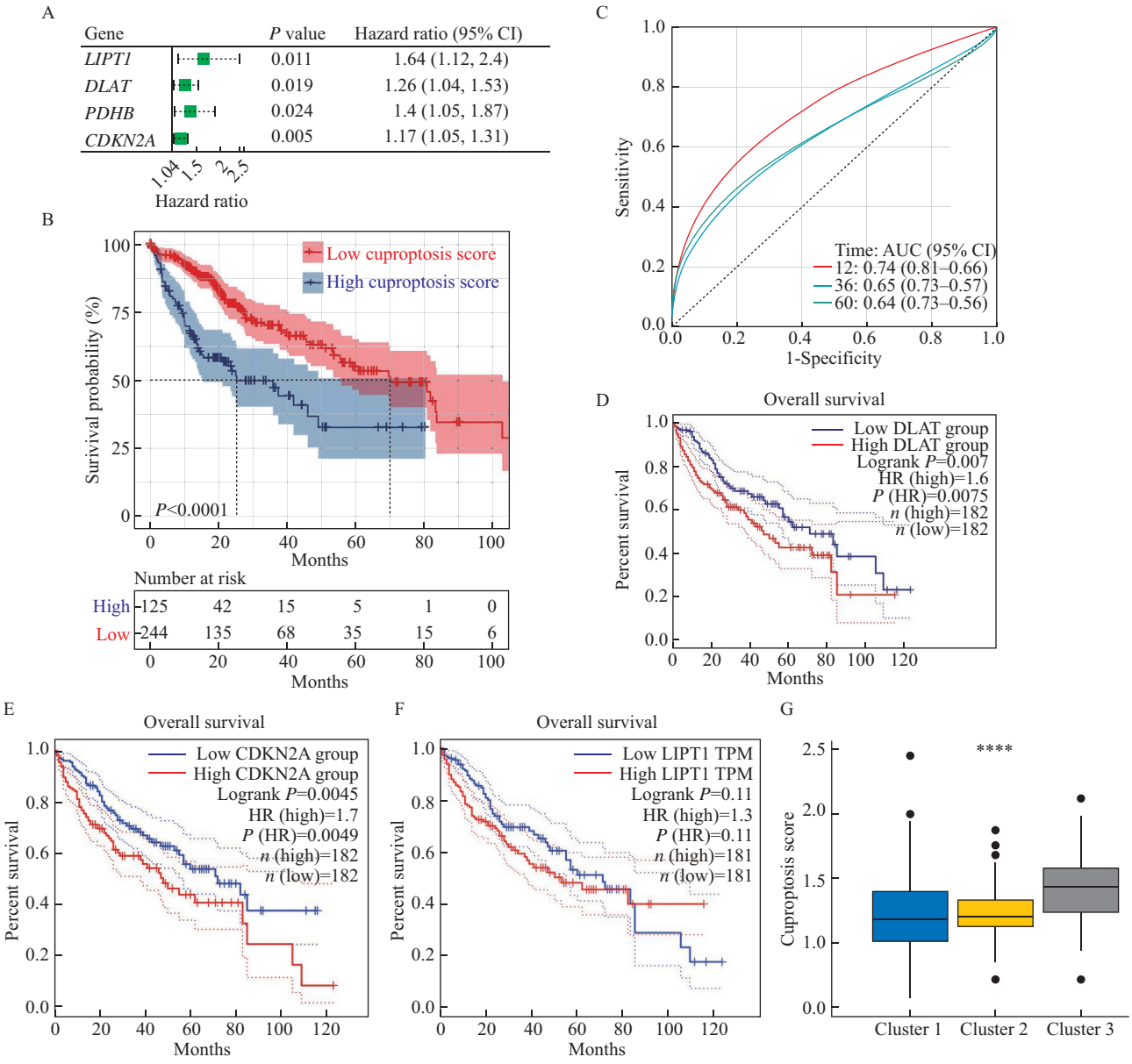


**Fig. 3** Association between cuproptosis score and prognosis of hepatocellular carcinoma (HCC)

A: forest map of univariate Cox analysis based on cuproptosis-related genes (CRGs); B: Kaplan-Meier curves were used to analyze the survival probability of patients with high (125 cases) and low (244 cases) cuproptosis scores in The Cancer Genome Atlas (TCGA) cohorts; C: the predictive value of cuproptosis score in 1-, 3- and 5- survival of patients with HCC with AUC of 0.74, 0.65, and 0.64, respectively. Kaplan-Meier curves showing overall survival (OS) of HCC patients with high and low expression of DLAT (D), CDKN2A (E), and LIPT1 (F); G: the distribution of cuproptosis score in different cuproptosis clusters. The statistical differences among the three clusters were analyzed by the kruskal test. $^{*}P<0.05$, $^{**}P<0.01$, $^{***}P<0.001$, $^{****}P<0.0001$; ns: not statistically significant

establish the cuproptosis signature based on the 4 CRGs. According to the optimal lambda value determined by the LASSO model (fig. S3A and S3B), 3 key genes (*LIPT1*, *DLAT*, *CDKN2A*) were identified. We report the relationship between different risk scores and follow-up time, events and changes in CRG expression in fig. S3D. A cuproptosis prognostic signature was then established and defined as the cuproptosis score. According to a cutpoint of 1.39 (fig. S3C), 369 patients with HCC were divided into high cuproptosis score ($n$=125) and low cuproptosis score ($n$=244) groups. The low cuproptosis score group showed a survival advantage in the TCGA cohorts (fig. 3B). We next drew the ROC curves for the cuproptosis prognostic signature (fig. 3C). The ROC curve revealed that the cuproptosis signature was effective in predicting the 1-, 3-, and 5-year survival rate of HCC patients. High expression of DLAT and CDKN2A was correlated with poor prognosis (fig. 3D and 3E), but the expression of LIPT1 did not affect overall survival (fig. 3F). We also found that the cuproptosis score was an independent prognostic factor for HCC with a significantly higher hazard ratio (HR, 2.72) (fig. 4A). Thus, we propose that the cuproptosis prognostic signature is a better predictor of prognosis than individual key gene.

Next, the relationship between the cuproptosis score and cuproptosis clusters 1–3 was further explored. Cluster 3 with poor prognosis had a high cuproptosis score, while cluster 2 with better prognosis had a low cuproptosis score (fig. 3G), further proving that the cuproptosis prognostic signatures are indicative of prognosis of HCC. Despite a higher expression level of immune checkpoint blockade (ICB) in the high cuproptosis score group (fig. 4B), there was no ICB therapy response difference between high and low cuproptosis score groups (fig. S3E), suggesting that better prognosis of patients with low cuproptosis score may not be related to efficacy of ICB therapy. This further indicated a higher proportion of patients with lower stage and grade in the low cuproptosis score groups (fig. 4C and 4D). This result was mutually corroborated by the survival analysis. Subsequently, the infiltration of 27 kinds of TME immune cells was further studied in the high and low cuproptosis score groups. In the high cuproptosis score group, immune cells involved in tumor immune activation were infiltrated more (fig. 4E). Meanwhile, the expression levels of CDKN2A, DLAT, and LIPT1 were positively associated with the immune infiltration level (fig. S4A–S4C).

### 2.4 Exploration of Role of Three Key CRGs in Cuproptosis of HCC

To validate the associations of the expression levels of three hub genes with HCC, we performed an expression analysis using Gene Expression Profiling Interactive Analysis 2 (GEPIA2) and UALCAN based on TCGA samples. CDKN2A, DLAT, and LIPT1 were highly expressed in the tumor compared to normal samples (fig. 5A–5F) and positively correlated with clinical stage and grade (fig. 5G and 5L). Western blotting and qRT-PCR revealed that DLAT was highly expressed in multiple liver cancer cell lines, but LIPT1 and CDKN2A were not (fig. 6A–6D). Moreover, DLAT was also highly expressed in 40 pairs of HCC tissues compared to adjacent normal tissues by Western blotting and qRT-PCR (fig. 6E–6H). This result is consistent with immunohistochemistry (IHC) results (fig. 6J). However, the mechanism was unclear. To experimentally explore the role of DLAT in cuproptosis in HCC, we added potent copper ionophore elesclomol to increase intracellular copper levels of MHCC-97H and demonstrated that elesclomol caused a decrease of cell viability (fig. 7A and 7B). Ammonium tetrathiomolybdate (TTM) is a kind of selective $Cu^{++}$ chelator that reduces intracellular copper by chelating intracellular copper ions. We found that the addition of TTM almost completely prevented the cytotoxic effects induced by elesclomol (fig. 7C). Western blotting and qRT-PCR results showed that the expression levels of DLAT were elevated when HepG2 and PLC/PRF/5 cells were treated with elesclomol (fig. 7D–7F). When the expression of DLAT was reduced by siRNA (fig. 7G and 7H), we observed recovery of elesclomol-induced cuproptosis of PLC/PRF/5 cells (fig. 7I). Finally, we found no significant difference in the proliferative activity in PLC and MHCC-97H cells (fig. 7J).

## 3 DISCUSSION

In recent years, advances in both traditional systemic regimens and emerging immunotherapy strategies have been reported, yet knowledge about the sensitivity of drug therapy remains limited[19]. Accurate identification of the molecular subtypes of HCC is therefore essential to guide individualized treatment. Cuproptosis, a nonapoptotic cell death pathway, may be a potential candidate for clinical application and treatment for a variety of human cancers[29]. In many respects, cuproptosis is still in its infancy and urgently demands further research.

In the present study, we found that cluster 2 exhibited a significant survival advantage among three cuproptosis clusters. We assessed the correlations between three cuproptosis clusters and TME cell infiltration. However, the role of immune cells in the TME is complex. According to the results of ssGSEA analysis, cluster 2 was significantly associated with immune activation. These findings may advance our understanding of the relationship between cuproptosis, TME cell infiltration, and HCC. However, the relationship between cuproptosis and immunity needs further study.

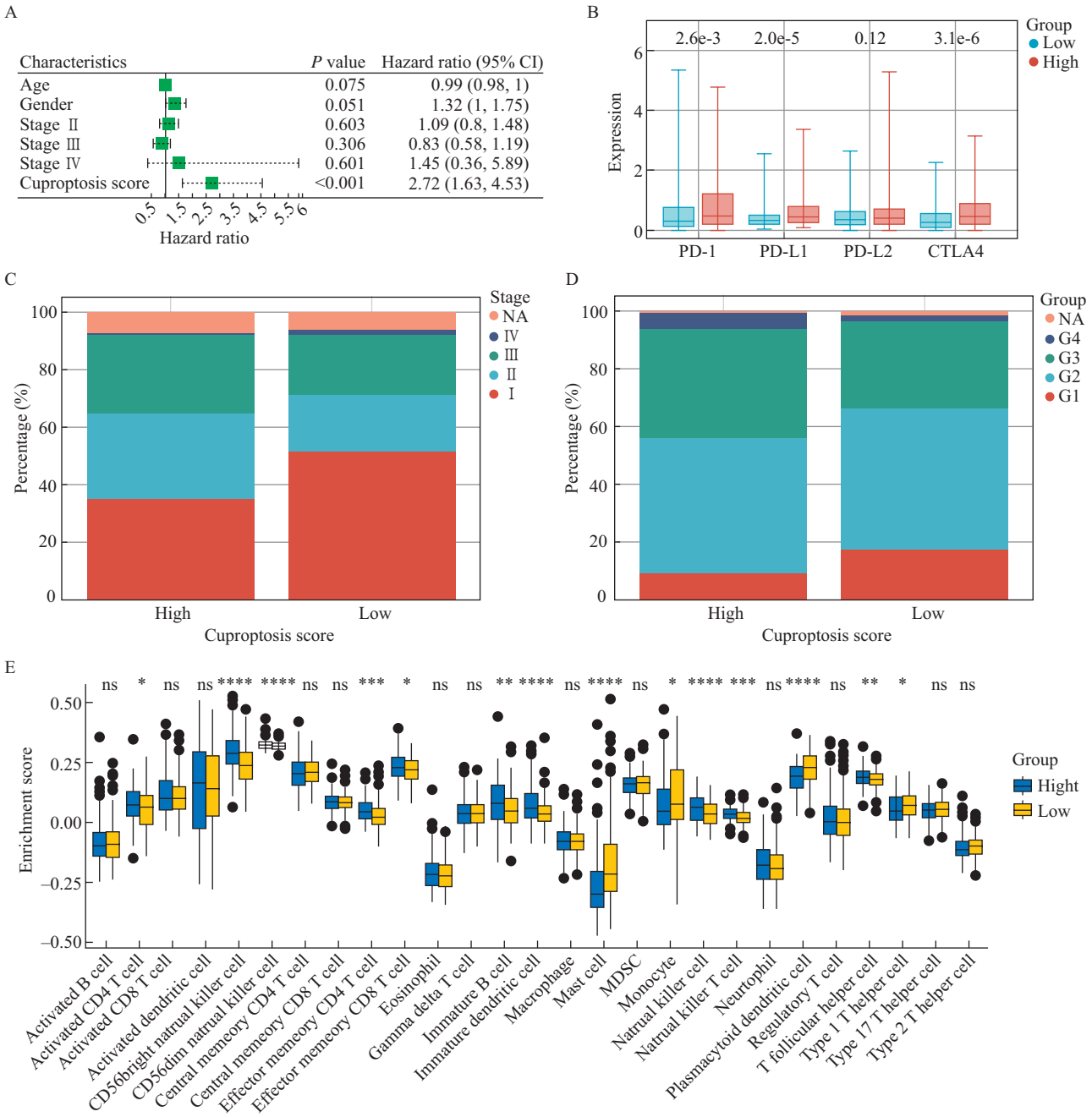


**Fig. 4** Characteristics of cuproptosis score in The Cancer Genome Atlas (TCGA) cohort

A: forest map of cuproptosis score and other clinicopathological parameters; B: differential expression of immune checkpoint related molecules in high and low cuproptosis score groups; C and D: proportions of stage (C) and grade (D) in high and low cuproptosis score groups; E: 27 tumor microenvironment (TME) cells infiltration abundance in high and low cuproptosis score groups. The statistical differences among the three clusters were analyzed by the kruskal test. $^{*}P<0.05$, $^{**}P<0.01$, $^{***}P<0.001$, $^{****}P<0.0001$; ns: not statistically significant; MDSC: myeloid derived suppressor cell

To explore whether CRGs are indicative of prognosis of HCC, we established a cuproptosis prognostic model based on the four CRGs associated with prognosis. A cuproptosis signature based on three key genes (*DLAT*, *CDKN2A* and *LIPT1*) was constructed to quantify cuproptosis scores. As shown in the results, the patients with a low cuproptosis score had an advantage of survival probability. Specifically, cluster 3 with poor prognosis was significantly correlated with a high cuproptosis score, and cluster 2 with better prognosis was significantly correlated with a low cuproptosis score. The cuproptosis signature was effective in predicting the 1-, 3-, and 5-year survival rates of HCC patients. Meanwhile, lower gene expression of single DLAT and CDKN2A had better prognosis. The HR of high expression group was 1.6 and 1.7, respectively. However, the cuproptosis score was an independent prognostic factor for HCC with a significantly higher HR (2.72). These indicated that the cuproptosis score is associated with a higher

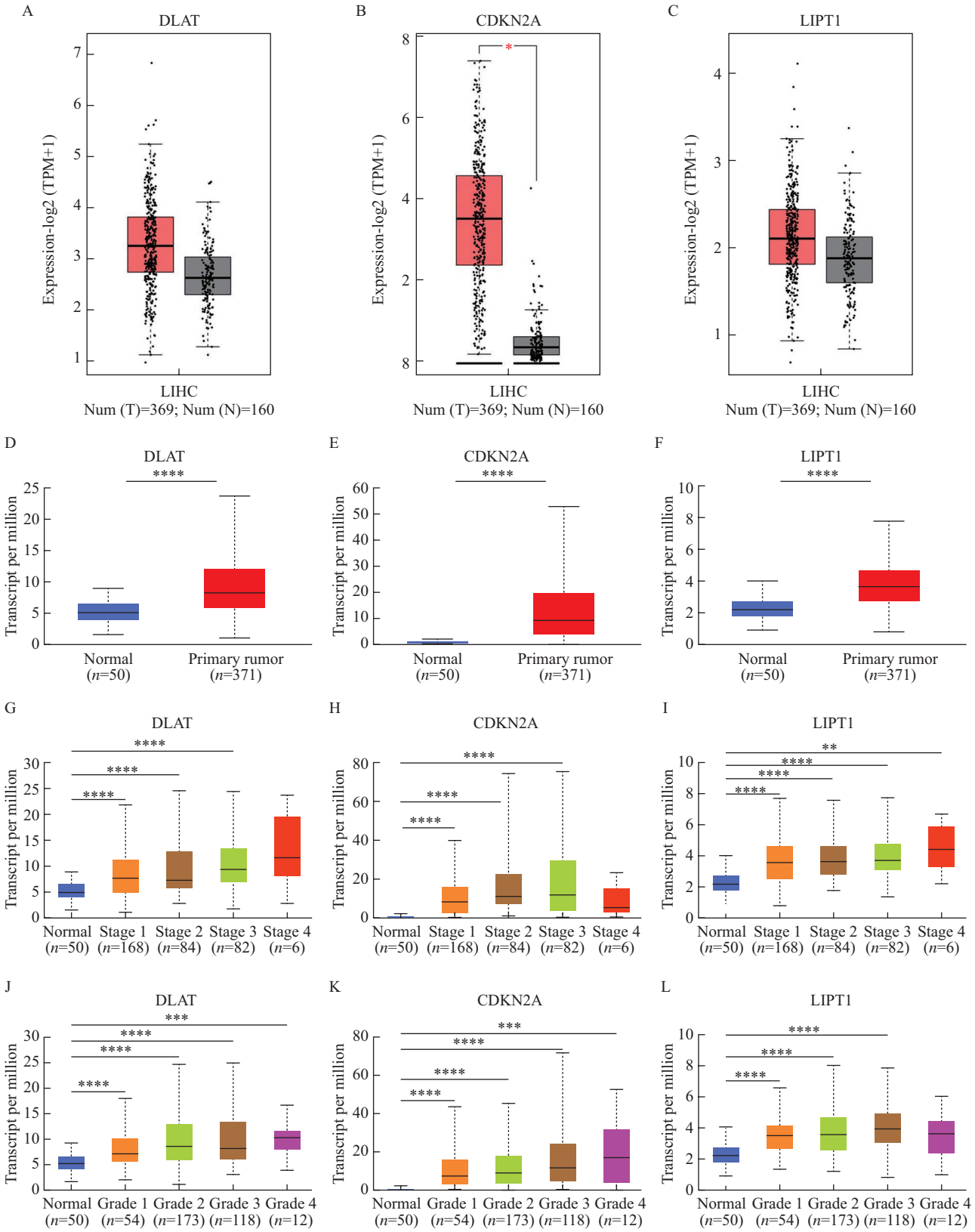


**Fig. 5** Expression of three hub genes and the relationship with clinicopathological features

A–C: boxplots of the expression of DLAT (A), CDKN2A (B) and LIPT1 (C) between tumor and normal samples in GEPIA2; D–F: boxplots of the expression of DLAT (D), CDKN2A (E), and LIPT1 (F) between tumor and normal samples in UALCAN; G–I: boxplots of the expression of DLAT (G), CDKN2A (H) and LIPT1 (I) between individual cancer stages in UALCAN; J–L: boxplots of the expression of DLAT (J), CDKN2A (K) and LIPT1 (L) between different tumor grades in UALCAN. LIHC: liver hepatocellular carcinoma, presented in TCGA database. $^{*}P<0.05$, $^{**}P<0.01$, $^{***}P<0.001$, $^{****}P<0.0001$; ns: not statistically significant

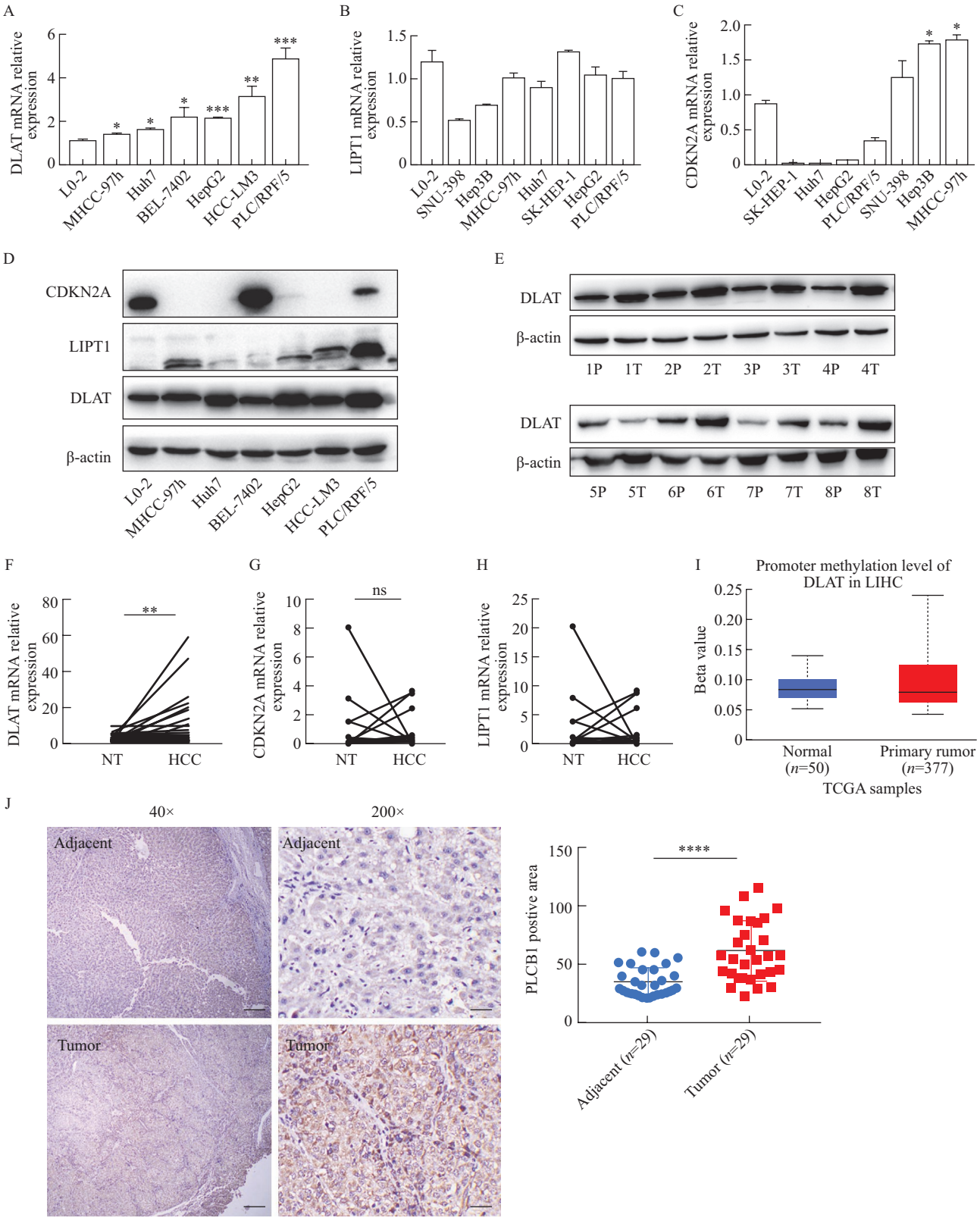


**Fig. 6** Expression level of three hub genes in cell lines and clinical tissues of hepatocellular carcinoma (HCC)
A: The mRNA expression levels of *DLAT* (A), *LIPT1* (B) and *CDKN2A* (C) were examined by SYBR Green qRT-PCR in normal hepatocytes (L0-2) and liver cancer cells; D: The protein levels of DLAT, LIPT1 and CDKN2A were examined by Western blotting in liver cancer cells (HMCC-97H, Huh7, BEL-7402, HepG2, HCC-LM3, PLC/PRF/5); E: The protein level of DLAT was examined by Western blotting in HCC tissues; F–H: The mRNA expression levels of *DLAT* (F), *CDKN2A* (G) and *LIPT1* (H) were examined by SYBR Green qRT-PCR in HCC tissues; I: promotor methylation level of DLAT in normal and HCC patients in UALCAN; J: typical immunohistochemical image of DLAT in adjacent liver tissues and HCC tissues. Scale bar (40×) = 500 μm; scale bar (200×) = 100 μm. LIHC: liver hepatocellular carcinoma, presented in TCGA database. $^{*}P<0.05$, $^{**}P<0.01$, $^{***}P<0.001$, $^{****}P<0.0001$; ns: not statistically significant

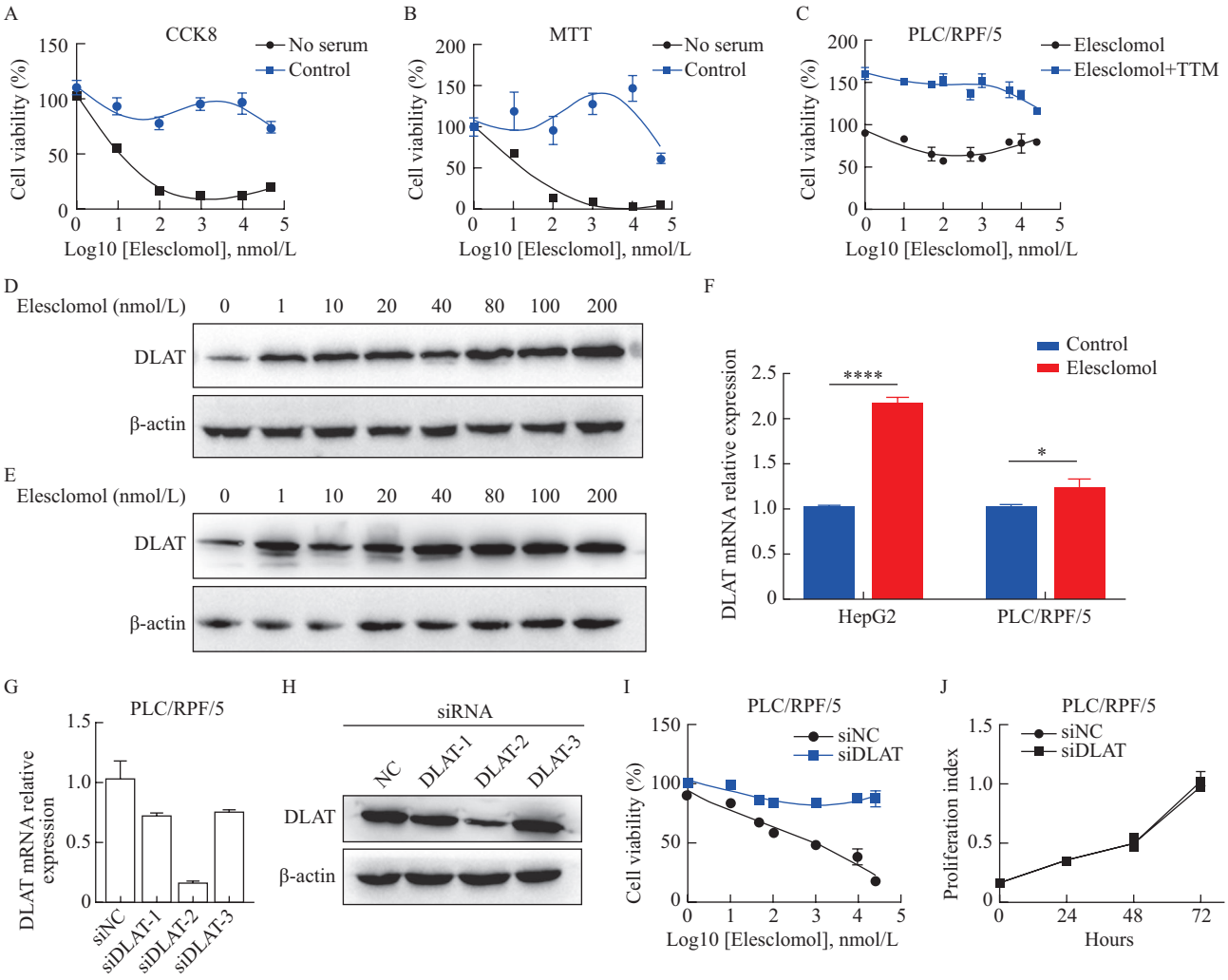


**Fig. 7** Function of DLAT in cuproptosis caused by elesclomol in hepatocellular carcinoma (HCC)
A and B: the relative cell viability of 97H cells when grown in the presence or absence of serum and treated with elesclomol by CCK8 assay (A) and MTT assay (B); C: the relative cell viability of 97H cells when grown in the presence or absence of TTM (10 μmol/L) and treated with indicated concentration of elesclomol; D and E: The protein expression levels of DLAT was detected by Western blotting in HepG2 cells (D) and PLC/PRF/5 cells (E) treated with indicated concentration of elesclomol for 48 h; F: The mRNA expression levels of DLAT were detected by SYBR Green qRT-PCR in HepG2 cells and PLC/PRF/5 cells treated with 80 nmol/L elesclomol for 48 h;. G and H: The mRNA (G) and protein (H) levels of DLAT were examined by SYBR Green qRT-PCR and Western blotting in PLC/PRF/5 cells after transfected with siRNA; I: The relative cell viability of PLC/PRF/5 cells treated with indicated concentration of elesclomol after transfection with siNC and siDLAT was tested by CCK8 assay; J: The relative cell viability was examined by CCK8 assay in PLC/PRF/5 cells after transfected with siDLAT and siNC. $^{*}P<0.05$, $^{**}P<0.01$, $^{***}P<0.001$, $^{****}P<0.0001$; ns: not statistically significant

risk of HCC. This suggests that the cuproptosis prognostic signature is a better predictor of prognosis than individual key genes and has potential as an independent prognostic biomarker in HCC patients. The pathological distribution results showed the cuproptosis score could also indicate the clinical grade and stage. These results are mutually corroborated by the results of the survival analysis.

To explore the role of three key CRGs in cuproptosis of HCC, we performed expression analysis using an online database and experimental validation. CDKN2A, DLAT, and LIPT1 were highly expressed in multiple liver cancer cell lines and HCC tissues compared to normal samples and positively correlated with clinical stage and grade. This reveals the role of *CDKN2A*, *DLAT*, and *LIPT1* as cancer promotor genes. The addition of elesclomol-induced cuproptosis in HCC, elevated DLAT expression, and reduced DLAT restored the viability of liver cancer cells. However, DLAT has no effect on the proliferation of liver cancer. The addition of the selective $Cu^{++}$ chelator, TTM, almost completely prevented the cytotoxic effects induced by elesclomol. This reveals that the cytotoxic effects induced by elesclomol are dependent on copper ions. Multiple studies have confirmed the anticancer effects of elesclomol, which is influenced by the metabolic environment of lung cancer, glioblastoma, and colorectal cancer[2, 30–32]. The literature suggests that

patients with low lactate dehydrogenase (LDH) levels associated with enhanced mitochondrial metabolism may be more sensitive to elesclomol[2, 33]. However, the role of elesclomol in the treatment of HCC is sorely lacking. Thus, our discovery of DLAT as an important target for cuproptosis may be an important treatment strategy against HCC. Furthermore, DLAT may be a prognostic marker, promising biomarker, and target for intervention in cuproptosis. Further *in vivo* and *in vitro* experimental studies are warranted to determine whether the cuproptosis prognostic signature and key cuproptosis genes play a critical role in HCC.

In conclusion, cuproptosis-related clusters depicted he TME heterogeneity. The cuproptosis score is a promising biomarker that could help determine the prognosis and molecular subtypes and may offer novel insights into the treatment of liver cancer. Specifically, elesclomol could act as an anticancer agent through DLAT in a copper-dependent manner.

**Conflict of Interest Statement**

The authors have no conflict of interest.

## REFERENCES


1 Cao M, Luo X, Wu K, *et al*. Targeting lysosomes in human disease: from basic research to clinical applications. Signal Transduct Target Ther, 2021,6(1):379
2 Tsvetkov P, Coy S, Petrova B, *et al*. Copper induces cell death by targeting lipoylated TCA cycle proteins. Science, 2022,375(6586):1254-1261
3 Lin S, Yang H. Ovarian cancer risk according to circulating zinc and copper concentrations: A meta-analysis and Mendelian randomization study. Clin Nutr, 2021,40(4):2464-2468
4 Xiao Y, Chen DI, Zhang X, *et al*. Molecular study on copper-mediated tumor proteasome inhibition and cell death. Int J Oncol, 2010,37(1):81-87
5 Blockhuys S, Celauro E, Hildesjö C, *et al*. Defining the human copper proteome and analysis of its expression variation in cancers. Metallomics, 2017,9(2):112-123
6 Ishida S, Andreux P, Poitry-Yamate C, *et al*. Bioavailable copper modulates oxidative phosphorylation and growth of tumors. Proc Natl Acad Sci USA, 2013,110(48): 19507-19512
7 Ge EJ, Bush AI, Casini A, *et al*. Connecting copper and cancer: from transition metal signalling to metalloplasia. Nat Rev Cancer, 2022,22(2):102-113
8 Zuo XL, Chen JM, Zhou X, *et al*. Levels of selenium, zinc, copper, and antioxidant enzyme activity in patients with leukemia. Biol Trace Elem Res, 2006,114(1-3):41-53
9 Lutsenko S. Human copper homeostasis: a network of interconnected pathways. Curr Opin Chem Biol, 2010,14(2):211-217
10 Jiang Y, Huo Z, Qi X, *et al*. Copper-induced tumor cell death mechanisms and antitumor theragnostic applications of copper complexes. Nanomedicine (Lond), 2022,17(5):303-324
11 Voli F, Valli E, Lerra L, *et al*. Intratumoral Copper Modulates PD-L1 Expression and Influences Tumor Immune Evasion. Cancer Res, 2020,80(19):4129-4144
12 Liao Y, Zhao J, Bulek K, *et al*. Inflammation mobilizes copper metabolism to promote colon tumorigenesis via an IL-17-STEAP4-XIAP axis. Nat Commun, 2020,11(1):900
13 Chan N, Willis A, Kornhauser N, *et al*. Influencing the Tumor Microenvironment: A Phase II Study of Copper Depletion Using Tetrathiomolybdate in Patients with Breast Cancer at High Risk for Recurrence and in Preclinical Models of Lung Metastases. Clin Cancer Res, 2017,23(3):666-676
14 Gupte A, Mumper RJ. Elevated copper and oxidative stress in cancer cells as a target for cancer treatment. Cancer Treat Rev, 2009,35(1):32-46
15 Yoshii J, Yoshiji H, Kuriyama S, *et al*. The copper-chelating agent, trientine, suppresses tumor development and angiogenesis in the murine hepatocellular carcinoma cells. Int J Cancer, 2001,94(6):768-773
16 Chen D, Cui QC, Yang H, *et al*. Disulfiram, a clinically used anti-alcoholism drug and copper-binding agent, induces apoptotic cell death in breast cancer cultures and xenografts via inhibition of the proteasome activity. Cancer Res, 2006,66(21):10425-10433
17 Karginova O, Weekley CM, Raoul A, *et al*. Inhibition of Copper Transport Induces Apoptosis in Triple-Negative Breast Cancer Cells and Suppresses Tumor Angiogenesis. Mol Cancer Ther, 2019,18(5):873-885
18 Sung H, Ferlay J, Siegel RL, *et al*. Global Cancer Statistics 2020: GLOBOCAN Estimates of Incidence and Mortality Worldwide for 36 Cancers in 185 Countries. CA Cancer J Clin, 2021,71(3):209-249
19 Luo XY, Wu KM, He XX. Advances in drug development for hepatocellular carcinoma: clinical trials and potential therapeutic targets. J Exp Clin Cancer Res, 2021,40(1):172
20 Lv H, Liu X, Zeng X, *et al*. Comprehensive Analysis of Cuproptosis-Related Genes in Immune Infiltration and Prognosis in Melanoma. Front Pharmacol, 2022,13:930041
21 Chen Q, Wang Y, Yang L, *et al*. PM2.5 promotes NSCLC carcinogenesis through translationally and transcriptionally activating DLAT-mediated glycolysis reprograming. J Exp Clin Cancer Res, 2022,41(1):229
22 Goh WQ, Ow GS, Kuznetsov VA, *et al*. DLAT subunit of the pyruvate dehydrogenase complex is upregulated in gastric cancer-implications in cancer therapy. Am J Transl Res, 2015,7(6):1140-1151
23 Stone S, Jiang P, Dayananth P, *et al*. Complex structure and regulation of the P16 (MTS1) locus. Cancer Res, 1995,55(14):2988-2994
24 Song W, Ren J, Xiang R, *et al*. Identification of pyroptosis-related subtypes, the development of a prognosis model, and characterization of tumor microenvironment infiltration in colorectal cancer. Oncoimmunology, 2021,10(1):1987636
25 Kim Y, Kang JW, Kang J, *et al*. Novel deep learning-based survival prediction for oral cancer by analyzing tumor-infiltrating lymphocyte profiles through CIBER-SORT. Oncoimmunology, 2021,10(1):1904573
26 Wang T, Dai L, Shen S, *et al*. Comprehensive Molecular Analyses of a Macrophage-Related Gene Signature With Regard to Prognosis, Immune Features, and Biomarkers

for Immunotherapy in Hepatocellular Carcinoma Based on WGCNA and the LASSO Algorithm. Front Immunol, 2022,13:843408
27 Tang Z, Kang B, Li C, *et al*. GEPIA2: an enhanced web server for large-scale expression profiling and interactive analysis. Nucleic Acids Res, 2019,47(W1):W556-W560
28 Li T, Fan J, Wang B, *et al*. TIMER: A Web Server for Comprehensive Analysis of Tumor-Infiltrating Immune Cells. Cancer Res, 2017,77(21):e108-e110
29 Li SR, Bu LL, Cai L. Cuproptosis: lipoylated TCA cycle proteins-mediated novel cell death pathway. Signal Transduct Target Ther, 2022,7(1):158
30 Buccarelli M, D′Alessandris Q, Matarrese P, *et al*. Elesclomol-induced increase of mitochondrial reactive oxygen species impairs glioblastoma stem-like cell survival and tumor growth. J Exp Clin Cancer Res, 2021,40(1):228
31 Wangpaichitr M, Wu C, You M, *et al*. N′,N′-Dimethyl-N′,N′-bis(phenylcarbonothioyl) Propanedihydrazide (Elesclomol) Selectively Kills Cisplatin Resistant Lung Cancer Cells through Reactive Oxygen Species (ROS). Cancers (Basel), 2009,1(1):23-38
32 Gao W, Huang Z, Duan J, *et al*. Elesclomol induces copper-dependent ferroptosis in colorectal cancer cells via degradation of ATP7A. Mol Oncol, 2021,15(12): 3527-3544
33 O′Day S, Eggermont A, Chiarion-Sileni V, *et al*. Final results of phase Ⅲ SYMMETRY study: randomized, double-blind trial of elesclomol plus paclitaxel versus paclitaxel alone as treatment for chemotherapy-naive patients with advanced melanoma. J Clin Oncol, 2013,31(9):1211-1218

(Received Nov. 9, 2022; accepted Mar. 24, 2023)